Characterization and Modeling of Polymeric Foam under Multi-Axial Static and Dynamic Loading

I. M. Daniel[1], J. S. Fenner[1], B. T. Werner[2] and J-M. Cho[3]

[1]Robert McCormick School of Engineering and Applied Science
Northwestern University, 2137 Tech Drive, Evanston, IL 60208, USA

[2]Sandia National Laboratories, Livermore, CA 94550, USA

[3]Hyundai Motor Co., Seoul, Korea

ABSTRACT

A polymeric foam commonly used in composite sandwich structures was characterized under multi-axial loading at strain rates varying from quasi-static to dynamic. Tests were conducted under uniaxial compression, tension, pure shear and combinations of normal and shear stresses. Quasi-static and intermediate strain rate tests were conducted in a servo-hydraulic testing machine. High strain rate tests were conducted using a split Hopkinson pressure bar (Kolsky bar) system made of polycarbonate bars having an impedance compatible to that of the foam material. The typical compressive stress-strain behavior of the polymeric foam exhibits a linear elastic region up to a yield point, a nonlinear elastic-plastic region up to an initial peak or "critical stress" corresponding to collapse initiation of the cells, followed by strain softening up to a local minimum (plateau or saddle point stress) and finally, a strain hardening region up to densification of the foam. The characteristic stresses of the stress-strain behavior vary linearly with the logarithm of strain rate. A general three-dimensional elastic-viscoplastic model, formulated in strain space, was proposed. The model expresses the multi-axial state of stress in terms of an effective stress, incorporates strain rate effects and includes the large deformation region. Stress-strain curves obtained under multi-axial loading at different strain rates were used to develop and validate the elastic-viscoplastic constitutive model. Excellent agreement was shown between model predictions and experimental results.

Keywords: A. Polymeric foams; B. Dynamic testing; B. Strain rate dependence; D. Constitutive modeling

1. Introduction

In many applications composite sandwich structures with polymeric foam cores are exposed to high energy and high velocity dynamic loadings producing multi-axial dynamic states of stress. They are commonly used as core materials in lightweight sandwich structures with high strength, stiffness and impact damage tolerance. The mechanical behavior of cellular foams has been investigated and extensively discussed in the literature [1-5]. However, characterization has been in general limited, and few of the models can capture all the characteristic features of structural foams subjected to multi-axial dynamic loads. Some foam materials, such as PVC foams (especially higher density ones), are strain rate dependent, anisotropic, and elastic/viscoplastic materials. Their deformation history during dynamic loading affects critically the integrity of the sandwich structure. Characterization and modeling of their behavior is especially challenging. Several studies have been reported on dynamic characterization of foams and the effect of strain rate [6-13]. Daniel and Rao characterized isotropic and anisotropic foams at strain rates up to 800 s^{-1} [8]. They used a Hopkinson bar system with polymeric (polycarbonate) rods for the high strain rate tests. Ouellet et al. conducted tests over a wider range of strain rates (0.0087-2,500 s^{-1}) and modeled the strain rate behavior [11]. More recent studies by Tagarielli et al. [12], Lee et al. [13] and Daniel and Cho [14] also covered a wide range of strain rates. Constitutive modeling over the wide range of strains and strain rates experienced by foams has lagged because of the finite deformations and the anisotropy involved in some foams, with few works reported in the literature [15-17]. This study expands previous ones to dynamic biaxial stress fields.

2. Material Characterization

The quasi-static characterization of this material was discussed previously by the authors [14]. The material studied was a closed cell PVC foam, Divinycell H250 (DIAB Inc.). The cell microstructure is shown in Fig. 1. On a macroscopic scale, the material is orthotropic/transversely isotropic with principal axes as shown in Fig. 1. Typical stress-strain curves of this material under tension and compression along principal material directions are shown in

Fig. 2. A typical foam stress-strain curve exhibits several stages of deformation , a linear elastic region up to the proportional limit (or yield point), a plastic region up to a peak or critical stress, a plateau region followed by "strain hardening" and culminating in global densification. The linear elastic behavior is associated with elastic bending or stretching of the cell walls; the local peak or "critical point" is related to initiation of cell collapse under wall buckling and/or plastic hinge formation; the plateau region is caused by continuing cell collapse and local densification (locked-up); the strain hardening region ends with the final densification stage which corresponds to complete cell collapse and touching of opposite cell walls.

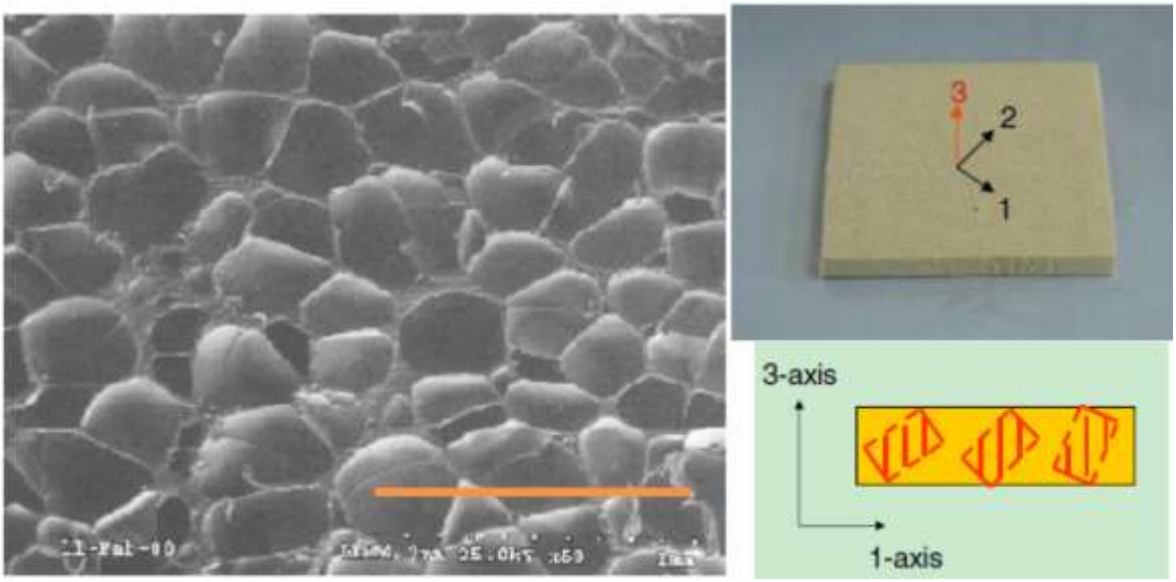

Fig. 1. Cell morphology of divinycell H250 foam (scale bar is 1 mm) and principal material axes of foam plate.

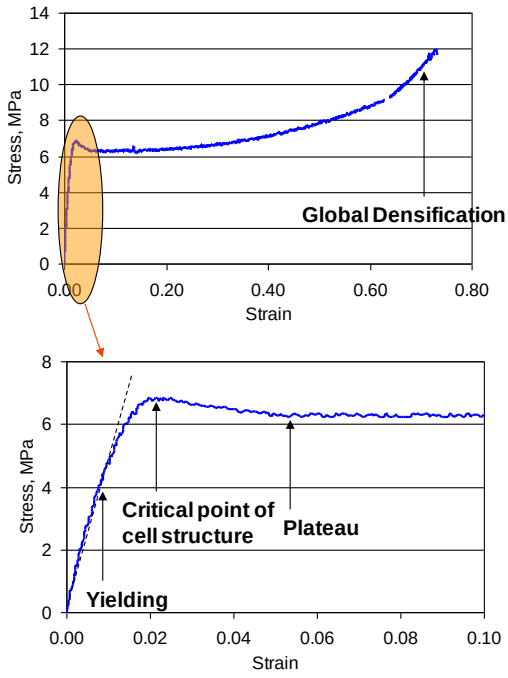

Fig. 2. Typical stress-strain curve and characteristic features of a foam under uniaxial compression

Macroscopic characterization of cellular foams is a challenging problem because of their hyperelastic behavior and tendency for deformation localization due to local collapse of cells and end crushing under compression. Some of the difficulties can be overcome by using stress-controlled and strain-controlled experiments and full-field strain measurement methods [14, 17]. Stress controlled experiments at various orientations with respect to the principal material axes were conducted with coupons of appropriate aspect ratio.

Strain controlled experiments were conducted by using thin plate specimens constrained between metal blocks as shown in Fig. 3. Such experiments were conducted at quasi-static and moderate strain rates of 10^{-4} and 1 s^{-1}. The optimum specimen aspect ratio for compressive, shear and combined compressive and shear strain loading was determined by Finite Element Analysis using previously published properties of a different batch of the same material [2]. The higher the aspect ratio the more homogeneous is the state of strain. An aspect ratio of 10 was deemed suitable for compression and shear specimens.

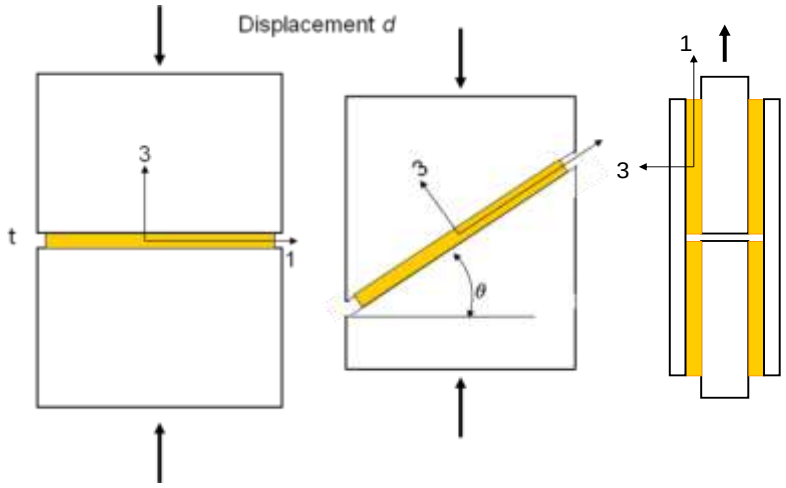

Fig. 3. Uniaxial, shear and biaxial strain experiments

Compressive stress-strain curves for the off-axis specimens tested under uniaxial stress are shown in Fig. 4 at various orientation with respect to the in-plane direction (1- or 2 -direction).. The effect of anisotropy is reflected in the variation in axial modulus and characteristic first peak in the stress-strain curve. The latter, as mentioned before, is the "critical point" of initiation of local collapse of the cell structure.

Compressive stress tests along the in-plane (1) and through-thickness (3) directions were conducted under uniaxial strain at three strain rates, quasi-static ($1\text{-}5 \times 10^{-4}$ s^{-1}), intermediate (1-3 s^{-1}) and high ($10^{3} s^{-1}$). Shear stress tests, were conducted with the shear test configuration of Fig. 3, at quasi-static and intermediate strain rates. Quasi-static and intermediate rate tests were conducted in a servo-hydraulic testing machine; high rate tests were conducted in a split Hopkinson (Kolsky) Pressure Bar (SHPB) system using polycarbonate bars for better impedance match with the foam material [14, 17]. All strain components other than the one measured were constrained to be zero. These tests yield the stiffness components $C_{11} = C_{22}$, C_{33}, $C_{44} = C_{55}$ and C_{66}.

Biaxial strain tests were conducted by the fixture shown in Fig. 3 under quasi-static and intermediate strain rate loadings. In these tests only the vertical load and crosshead displacement were recorded during the test. The strain components can be resolved from purely geometrical considerations as shown in Fig. 5. However, the stress components are more difficult to resolve because of the indeterminacy caused by the constraint on the loaded faces of the fixture and the unknown horizontal force components at these faces.

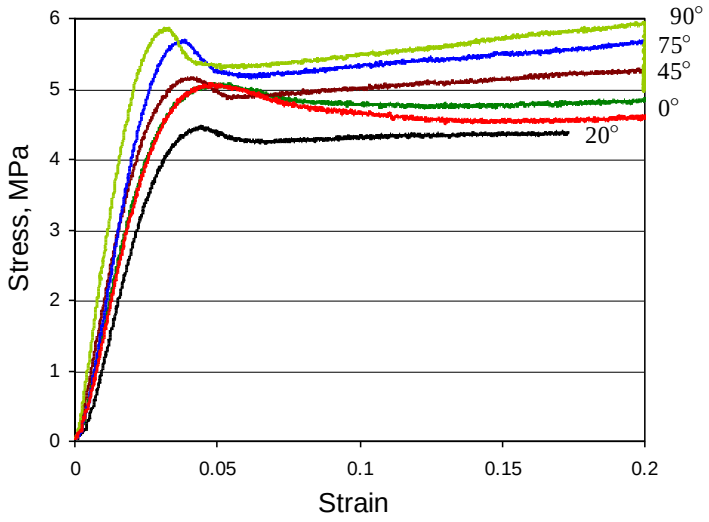

Fig. 4. Compressive stress-strain curves of off-axis specimens for loading orientations of 0, 20, 45, 70, and 90 deg with the 1-2 plane.

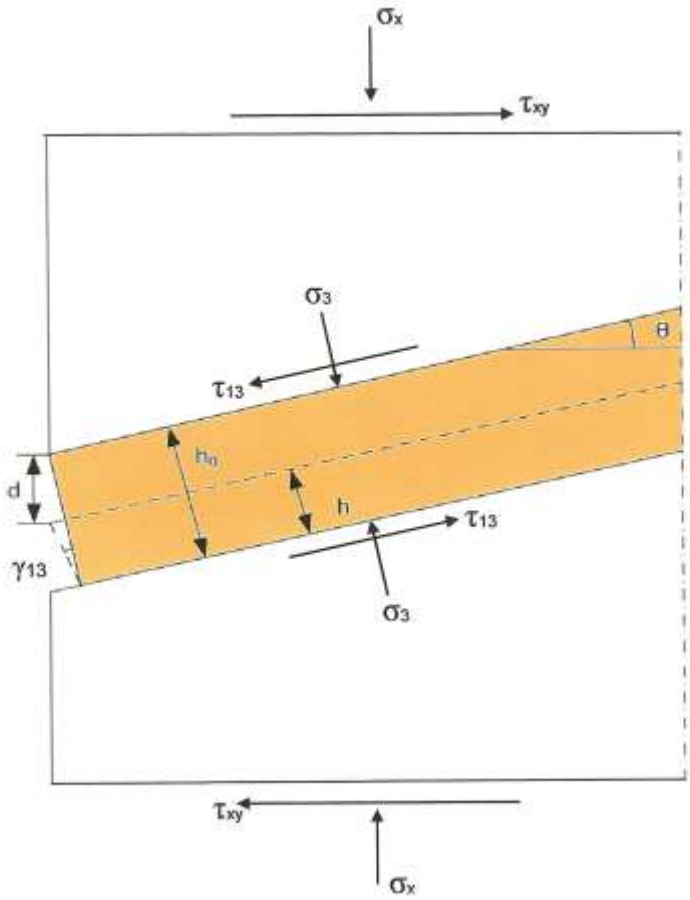

Fig. 5. Stresses and strains generated in biaxially loaded specimen under vertical displacement control

The engineering strains are

$$\varepsilon_3 = \frac{d}{h_o}\cos\theta,\ \varepsilon_1 = \varepsilon_2 = 0 \tag{1}$$

$$\gamma_{13} = \tan^{-1}\frac{d\sin\theta}{h_o - d\cos\theta} = \tan^{-1}\frac{\varepsilon_3\tan\theta}{1-\varepsilon_3}, \gamma_{12} = \gamma_{23} = 0, \tag{2}$$

The stresses are expressed as follows

$$\sigma_3 = \sigma_x - \tau_{13}\tan\theta = \sigma_x\cos^2\theta + \tau_{xy}\sin\theta\cos\theta \tag{3}$$

$$\tau_{13} = \sigma_3\tan\theta - \tau_{xy} = \sigma_x\sin\theta\cos\theta - \tau_{xy}\cos^2\theta \tag{4}$$

The experiments described before provide σ_x, θ, ε_3 and γ_3 and the experimental stress-strain relation

$$\tau_{13} = f(\gamma_{13}) \tag{5}$$

3. Strain-rate-dependent stress-strain behavior

Stress-strain curves obtained at strain rates ranging from $5\text{x}10^{-4}$ to $2\text{x}10^{3}$ s^{-1} under nearly homogeneous uniaxial compressive strain in the in-plane and through-thickness directions (1-and 3-directions, respectively) are shown in Figs. 6 and 7. The stiffness, based on the initial slope of these stress-strain curves, does not vary with strain rate. Four characteristic properties were identified in these stress-strain curves: 1) Yield stress, 2) Peak or "critical" stress corresponding to collapse initiation of the cells, 3) Plateau stress following the initial collapse of the cells, and 4) Strain hardening stress at the end of the plateau region and before the onset of densification. All of the above characteristic stresses increase with strain rate along radial lines from the origin. This behavior is similar to that observed for the polymer matrix of composites [18]. It was also found that these characteristic stresses vary linearly with the logarithm of strain rate. They can be normalized by their values at the reference strain rate (10^{-4} s^{-1} in this case) as shown in Fig. 8 for the case of in-plane loading. This allows for any property at any train rate to be related to the corresponding property at the reference strain rate as follows:

$$P(\dot{\varepsilon}) = P(\dot{\varepsilon}_o)\left(m\log_{10}\frac{\dot{\varepsilon}}{\dot{\varepsilon}_o} + 1\right) \tag{6}$$

where

P = property (yield stress, critical stress, plateau stress, strain hardening stress)

m = 0.104

$\dot{\varepsilon}_o$ = reference strain rate (10^{-4} s^{-1})

Using the above relation, the stress and strain at any strain rate can be transformed into equivalent values at the reference strain rate by the following transformation relations

$$\sigma^*(\dot{\varepsilon}_0) = \frac{\sigma(\dot{\varepsilon})}{K}$$
$$\varepsilon^*(\dot{\varepsilon}_0) = \frac{\varepsilon(\dot{\varepsilon})}{K} \tag{7}$$

where $K = m\log\left(\frac{\dot{\varepsilon}}{\dot{\varepsilon}_o}\right) + 1$ and the stress-strain curves of Figs. 6 and 7 can be collapsed into the master curves of Figs. 9 and 10.

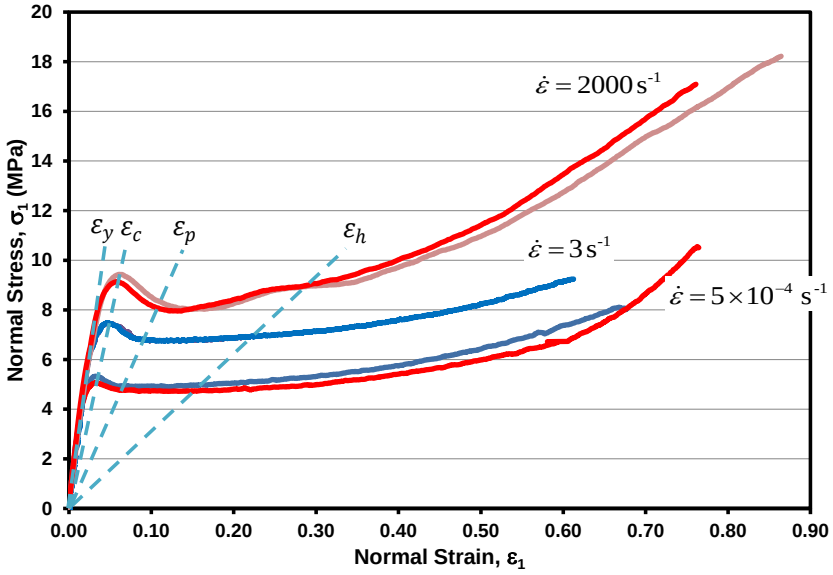

Fig. 6. Stress-strain curves at three strain rates (uniaxial strain along in-plane direction)

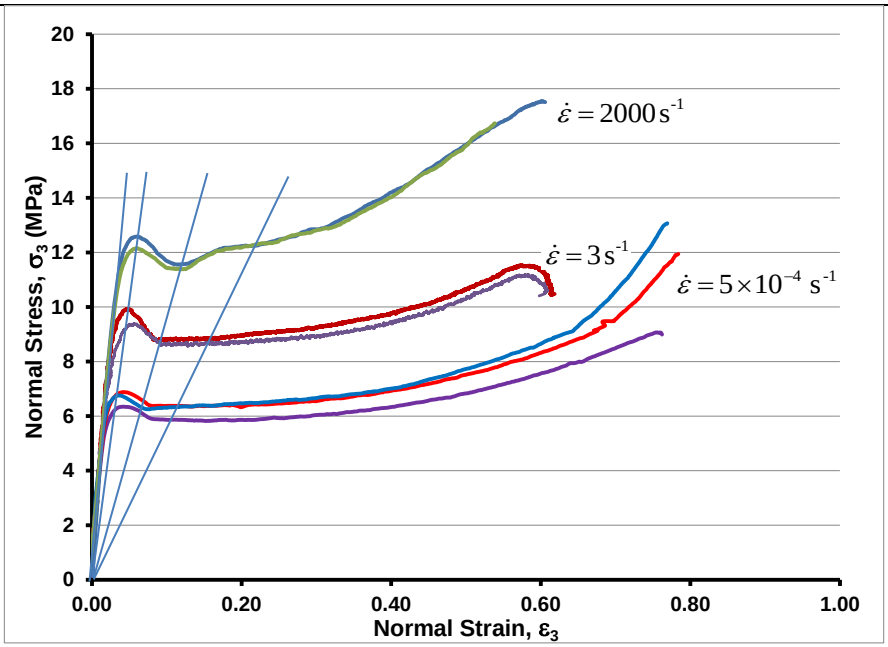

Fig. 7. Stress-strain curves at three strain rates (uniaxial strain in through-thickness direction)

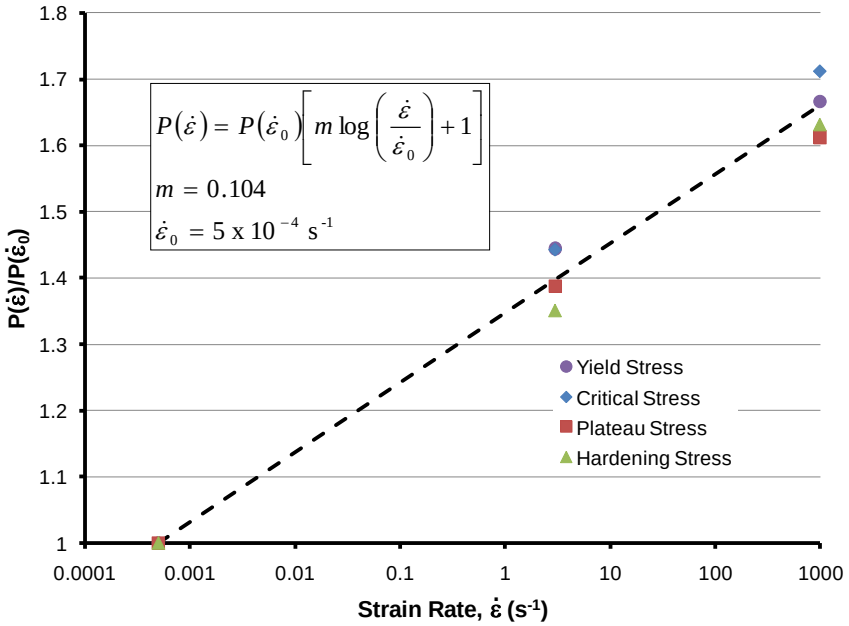

Fig. 8. Variation of normalized characteristic properties with strain rate for in-plane compressive loading

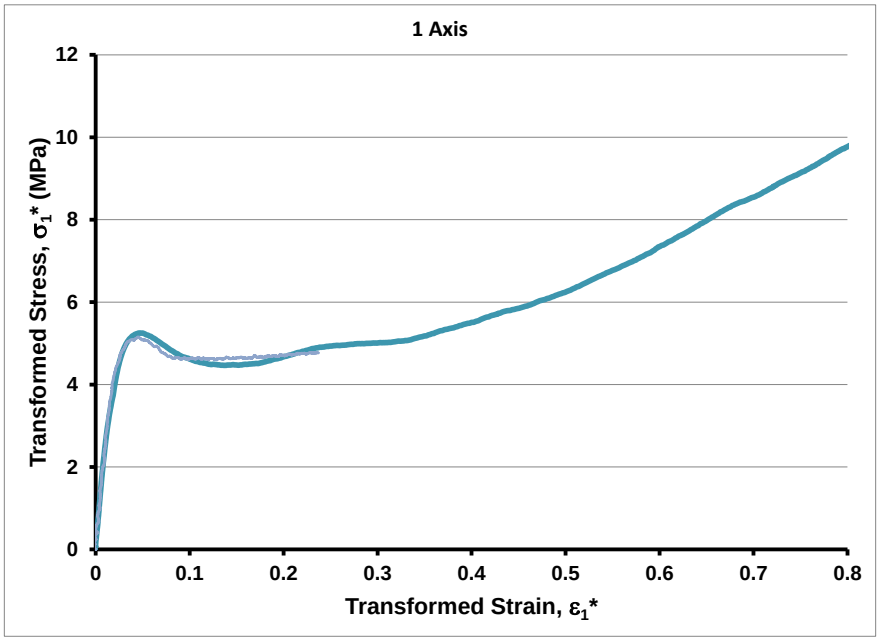

Fig. 9. Master stress-strain curve for in-plane compressive loading at any strain rate

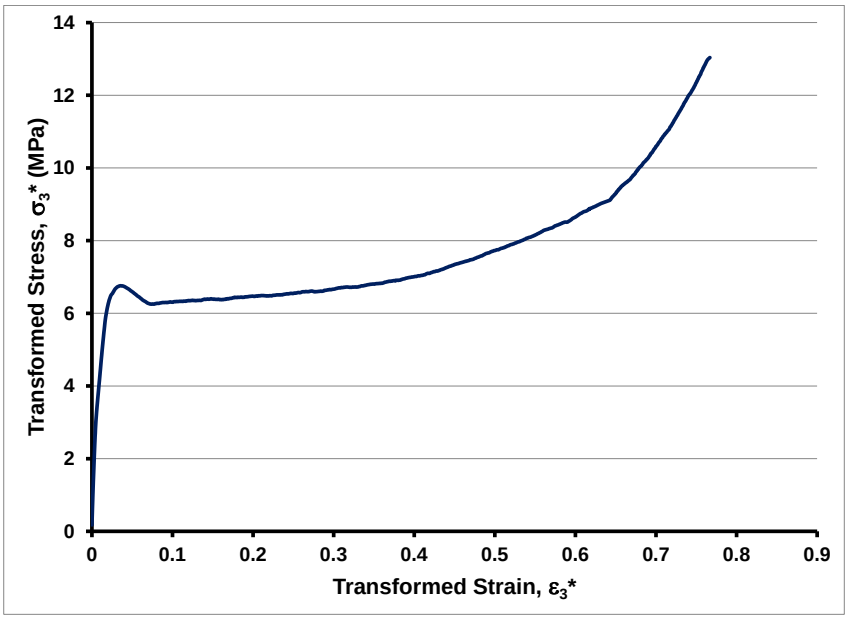

Fig. 10. Master stress-strain curve for through-thickness compressive loading at any strain rate

Stress-strain curves at two strain rates under in-plane and out-of-plane shear are shown in Figs. 11 and 12. Again, the yield stress and critical stress (as defined in Fig. 11) vary along radial lines through the origin linearly with the logarithm of strain rate. This allowed the representation of such curves by master stress-strain curves at the reference strain rate as shown if Fig. 13.

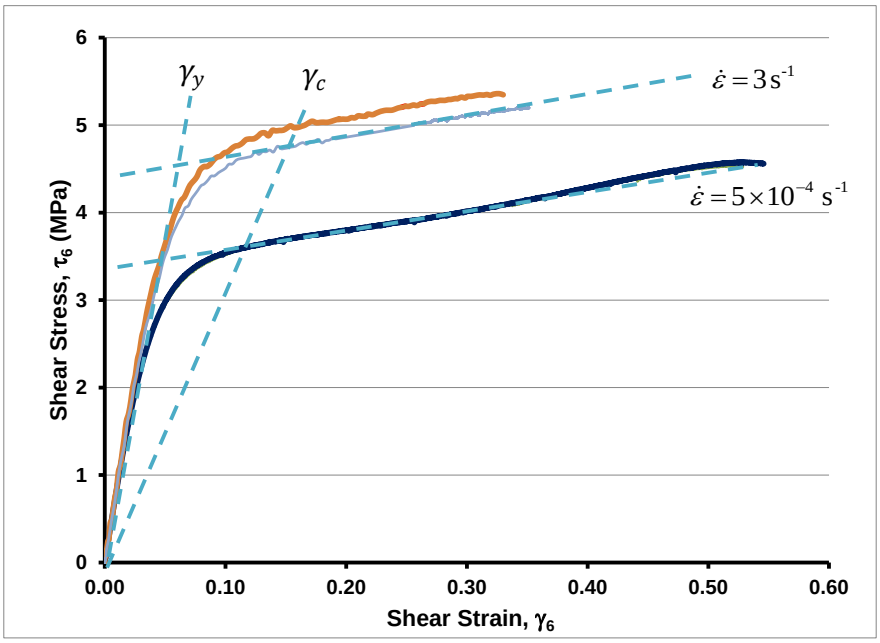

Fig. 11. Shear stress-strain curves at two strain rates (in-plane shear)

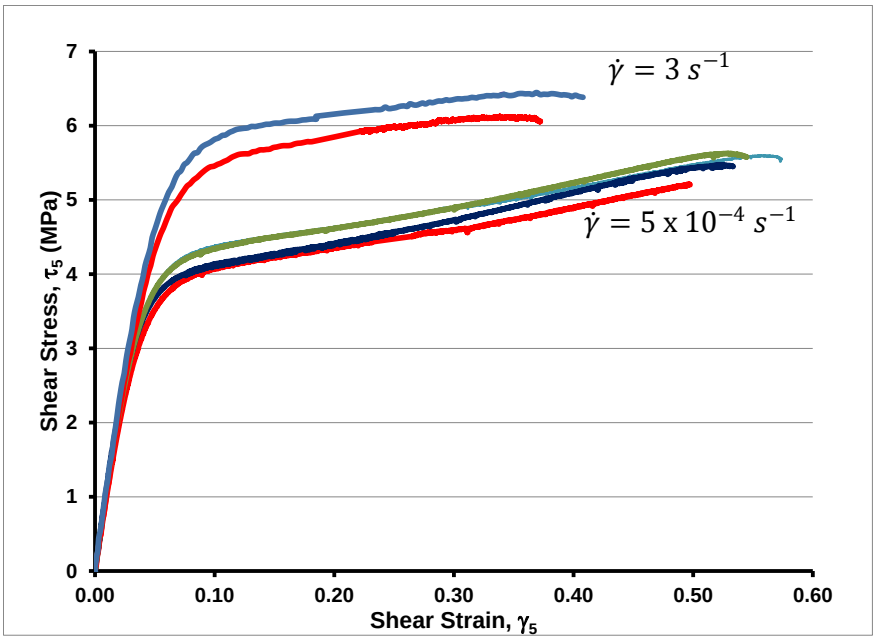

Fig. 12. Shear stress-strain curves at two strain rates (through-thickness shear)

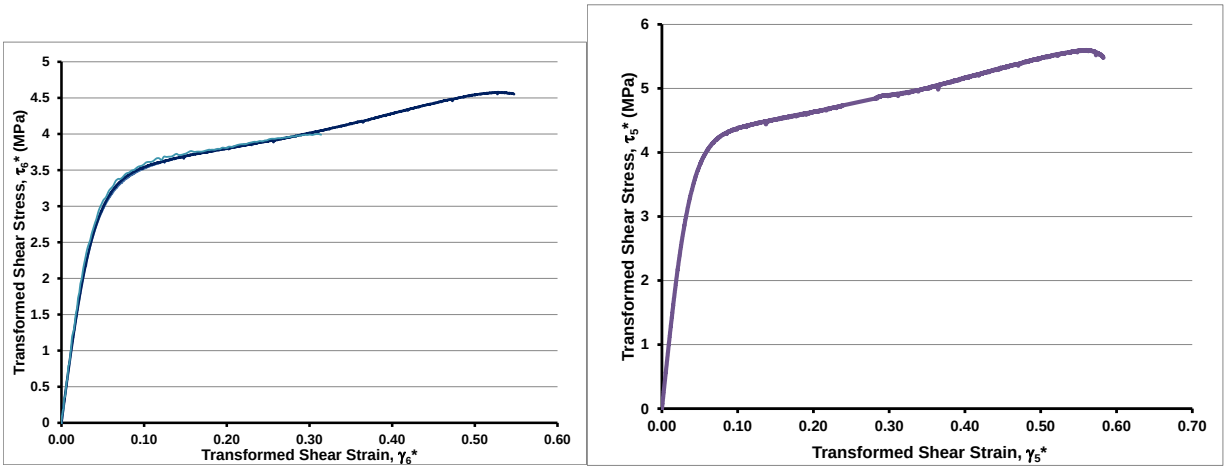

Fig. 13. Master shear stress-strain curves for in-plane shear (left) and through-thickness shear (right)

One characteristic feature in all stress-strain curves is the critical stress which was found to vary linearly with the logarithm of strain rate. This property for the various loadings and strain rates was normalized by its respective quasi-static (reference) value and plotted versus the logarithm of strain rate. It was seen that the normalized critical stress follows the same strain rate law for different loadings normal or shear, in-plane or through the thickness of the anisotropic foam material as was shown for the in-plane loading in Fig. 8.

Stress-strain curves at two strain rates, obtained from biaxial tests using the loading scheme of Fig. 3, are shown in Figs. 14-16. They represent combinations of compressive normal stress and out-of-plane shear stress. In the case of *20-deg loading, the behavior is dominated by the transverse compressive stress and the curves, for normal or shear* stress, show a pronounced critical peak. The curves for the 45-deg loading are equally influenced by the normal compressive and through-thickness shear stresses. The critical peaks are less pronounced. The case of 70-deg loading is dominated by the through-thickness shear behavior. The critical peaks are not distinct, as in the case of pure shear loading, because of the smooth transition from the elastoplastic regime to the strain hardening one. All critical stresses, after normalization by the quasi-static values, vary with strain rate like those discussed before for uniaxial loadings.

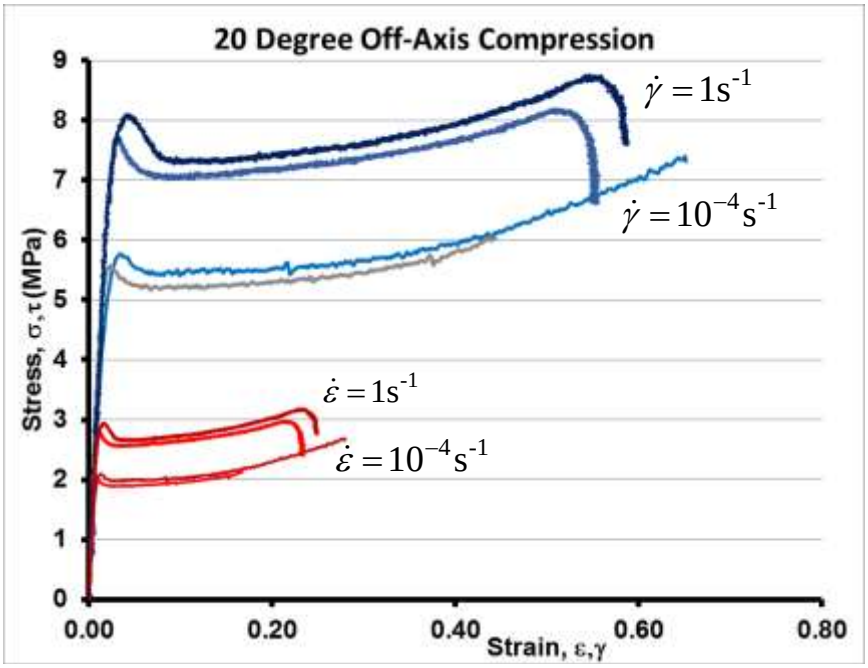

Fig. 14. Biaxial stress-strain curves obtained by loading at 20 deg with 3-direction

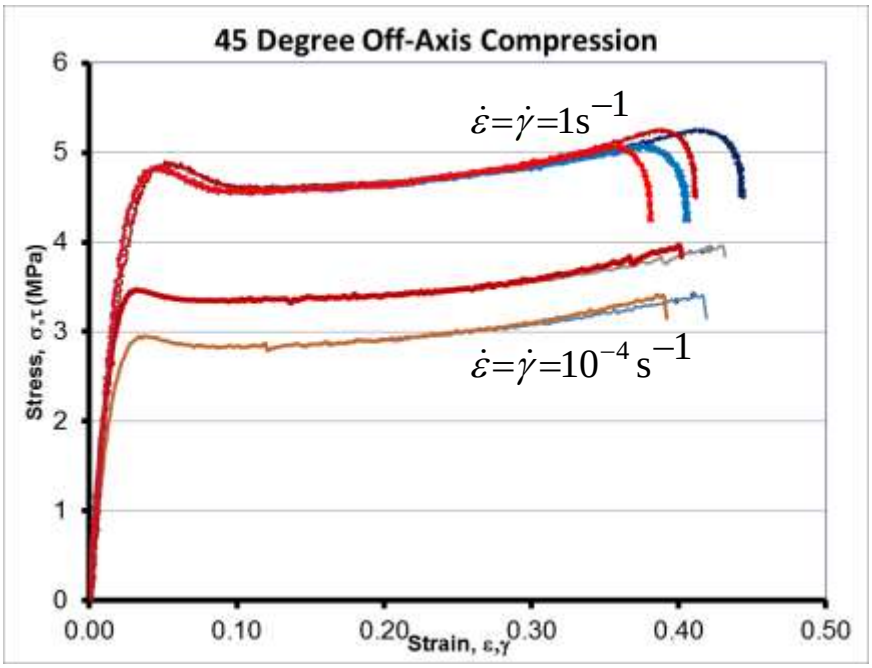

Fig. 15. Biaxial stress-strain curves obtained by loading at 45 deg with 3-direction

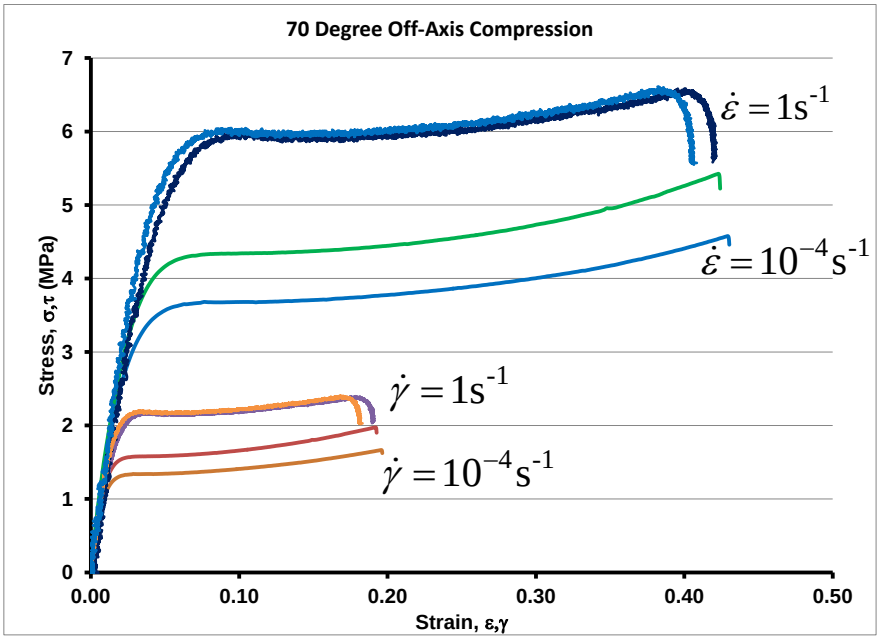

Fig. 16. Biaxial stress-strain curves obtained by loading at 70 deg with 3-direction

4. Constitutive Modeling

In the development above it was shown that the strain-rate dependence of the material behavior can be characterized by one parameter only, the slope *m* of the characteristic property versus logarithm of strain rate curve. Thus, modeling of the constitutive behavior at one strain rate (reference rate) would be sufficient to describe the mechanical behavior under any state of stress (or strain) and at any strain rate. The following loading function in strain space is proposed.

$$F = \left\{ \begin{array}{l} a_1(\varepsilon_1 - \varepsilon_2)^2 + a_2(\varepsilon_2 - \varepsilon_3)^2 + a_3(\varepsilon_3 - \varepsilon_1)^2 \\ + a_4(\gamma_4)^2 + a_5(\gamma_5)^2 + a_6(\gamma_6)^2 + a_v(\varepsilon_1 + \varepsilon_2 + \varepsilon_3)^2 \end{array} \right\}^{\frac{1}{2}} + b(\varepsilon_1 + \varepsilon_2 + \varepsilon_3) = \bar{\varepsilon} \tag{8}$$

where $F = \bar{\varepsilon}$ is the effective strain and $a_1, a_2, a_3, a_4, a_5, a_6, a_v, b$ are material parameters. The potential (loading) function consists of one part associated with deviatoric deformation including the terms with coefficients $a_1, a_2, a_3, a_4, a_5, a_6$, a quadratic dilatational term with coefficient a_v and a linear dilatational term with coefficient b. For a transversely isotropic material about the 3-axis

$$a_2 = a_3, \qquad a_6 = 2(2a_1 + a_3)$$

All stress-strain curves regardless of stress state or strain rate show similar elastic-plastic behavior up to the critical point. The linear elastic behavior is determined from the characterization tests described before which yielded the C_{ij} stiffness matrix. The plastic behavior has been represented before as a power law [17]. The combination of the linearelastic behavior and the power-law plastic behavior can be expressed in the following incremental constitutive relation

$$d\sigma_i = \left[C_{ij} - \left(nA(\bar{\varepsilon})^{n-1} \right) \frac{\partial F}{\partial \varepsilon_i} \frac{\partial F}{\partial \varepsilon_j} \right] d\varepsilon_j \tag{9}$$

For example, the stress-strain relation for the case of uniaxial loading in the 3-direction is modeled with a linear term for the linear elastic response and a power law term for the plastic deformation

$$\sigma_3 = C_{33}\varepsilon_3 - A{\varepsilon_3}^n \tag{10}$$

where C_{33} is the elastic stiffness and constants *A* an *n* are obtained in terms of the critical stress and critical strain [17].

A comparison with experimental results is shown in Fig. 17.

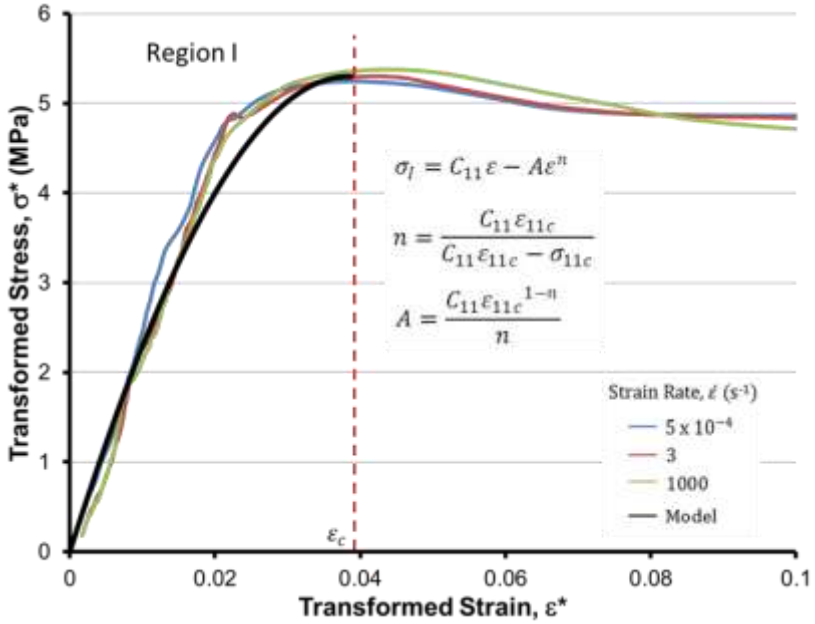

Fig. 17. Modeling of elasto-plastic stress-strain behavior for uniaxial loading in 3-direction

To predict the mechanical behavior of the material for any strain rate and any state of stress, the strain rate parameter *m*, the elastic constants of the material C_{ij}, the parameters of the potential function, and the power law curve fitting parameters *A* and *n* must be determined from experiments. The parameter *m* is determined from a few controlled tests at different (at least three) strain rates as discussed before. The material stiffnesses C_{ij} can be obtained by quasi-static (at the reference strain rate) characterization. The five independent parameters a_1, a_3, a_5, a_v, b can be determined by five independent quasi-static tests, e. g., tests in the 1- and 3-directions, two shear tests and a biaxial test.

5. Summary and Conclusions

An orthotropic polymeric cellular foam used in sandwich structures, was characterized under quasi-static and dynamic multiaxial loading conditions. The material investigated was a closed cell PVC foam, (Divinycell H250), having a density of 250 kg/m^3. Quasi-static (5×10^{-4} s^{-1}) and intermediate (3 s^{-1}) strain rate tests were conducted in a servo-hydraulic machine. High strain rate tests (10^3 s^{-1}) were conducted in a split Hopkinson (Kolsky) Pressure Bar (SHPB). This SHPB system was made of polymeric (polycarbonate) bars for closer impedance match with foam material.

Four characteristic properties were identified in the compressive stress-strain curves: 1) Yield stress, 2) Peak or "critical" stress corresponding to collapse initiation of the cells, 3) Plateau stress following the initial collapse of the cells, and 4) Strain hardening stress at the end of the plateau region and before the onset of densification. All of the above characteristic stresses vary linearly with the logarithm of strain rate. This allows for the development of a unified (master) stress-strain curve referred to one reference strain rate with the strain rate effect defined by a single parameter, the slope of the linear relation between properties and logarithm of strain rate. A constitutive model was proposed to describe the nonlinear multi-axial behavior based on a potential function in the form of a linear combination of deviatoric and dilatational deformation components.

Acknowledgements

The work described here was sponsored in part by the Office of Naval Research (ONR) and in part by the Department of Energy under a subcontract from the Ford Motor Company.

References

1. Gibson, L. J. and Ashby, M. F., Cellular solids, 2nd ed. New York: Cambridge University Press; 1997.
2. Daniel, I. M., Gdoutos, E. E., Wang, K. A. and Abot, J. L., Failure modes of composite sandwich beams. International Journal of Damage Mechanics 2002; 11: 309-334.
3. Gdoutos, E. E., Daniel, I. M. and Wang, K. A., Failure of cellular foams under multiaxial loading. Composites Part A 2002; 33:163-176.

4. Flores-Johnson, E. A., Li, Q. A., Degradation of elastic modulus of progressively crushable foams in uniaxial compression. Journal of Cellular Plastics 2008; 44: 415-434.
5. Abrate, S., Criteria for yielding or failure of cellular materials. Journal of Sandwich Structures and Materials 2008; 10: 5-51.
6. Ramon, O. and Mintz, J., Prediction of dynamic properties of plastic foams from constant strain rate measurements. J Appl Polym Scie 1990; 40(9-10):1683-1692.
7. Zhang, J., Lin, Z., Wong, A., Kikuchi, N., Li, V. C., Yee, A. F. and Nusholtz, G. S., Constitutive modeling and material characterization of polymeric foams. Journal of Eng. Materials and Technology 1997; 119: 284-291.
8. Daniel, I. M. and Rao, S., Dynamic mechanical properties and failure mechanisms of PVC foams. Dynamic Failure in Composite Materials and Structures, ASME Mechanical Engineering Congress and Exposition 2000; AMD-243:37-48.
9. Avalle, M., Belingardi, G. and Montanini, R., Characterization of polymeric structural foams under compressive impact loading by means of energy-absorption diagram. International Journal of Impact Engineering 2001; 25:455-472.
10. Viot, P., Beani, F. and Latallade, J. L., Polymeric foam behavior under dynamic compressive loading. J Mat Scie 2005; 40: 5829-5837.
11. Ouellet, S., Cronin, D. and Worswick, M., Compressive response of polymeric foams under quasi-static, medium and high strain rate conditions. Polymer Testing 2006; 25: 731-743.
12. Tagarielli, V. L., Deshpande, V. S. and Fleck, N. A., The high strain rate response of PVC foams and end-grain balsa wood. Composites Part B 2008; 39: 83-91
13. Lee, Y. S., Park, N. H. and Yoon, H. S., Dynamic mechanical characteristics of expanded polypropylene foams. J Cellular Plastics 2010; 46:43-55.
14. Daniel, I. M. and Cho, J. M., Characterization of anisotropic polymeric foam under static and dynamic loading. Experimental Mechanics 2011; 51(8):1395-1403.
15. Tagarielli, V. L., Deshpande, V. S., Fleck, N. A. and Chen, C., A constitutive model for transversely isotropic foams, and its application to the indentation of balsa wood. International Journal of Mechanical Sciences 2005; 47:666-686.
16. Gielen, A. W. J., A PVC-foam material model based on a thermodynamically elasto-plastic-damage framework exhibiting failure and crushing. International Journal of Solids and Structures 2008; 45:1896–1917.
17. Daniel, I. M., Cho, J. M. and Werner, B. T., Characterization and Modeling of Strain-Rate-Dependent Behavior of Polymeric Foams. Composites: Part A 2013; 45:70-78.
18. Werner, B. T. and Daniel, I. M., Characterization and modeling of polymeric matrix under static and dynamic loading. Composites Science and Technology 2014; 102:113-119.